



NIH PUBLIC ACCESS

Author Manuscript

*Mol Pharm.* Author manuscript; available in PMC 2013 June 04.

Published in final edited form as:

*Mol Pharm.* 2012 June 4; 9(6): 1705–1716. doi:10.1021/mp3000309.

## Prodrug Strategy for PSMA-targeted Delivery of TGX-221 to Prostate Cancer Cells

Yunqi Zhao<sup>a</sup>, Shaofeng Duan<sup>a</sup>, Xing Zeng<sup>b</sup>, Chunjing Liu<sup>c</sup>, Neal M. Davies<sup>d</sup>, Benyi Li<sup>b</sup>, and M. Laird Forrest<sup>a,\*</sup>

<sup>a</sup>Department of Pharmaceutical Chemistry, The University of Kansas, Simons Labs, 2095, Constant Ave. Rm. 136B, Lawrence, Kansas 66047, United States

<sup>b</sup>Department of Urology, The University of Kansas Medical Center, 3901 Rainbow Boulevard, Kansas City, Kansas 66160, United States

<sup>c</sup>Higuchi Biosciences Center, The University of Kansas, 2034 Becker Drive, Lawrence, Kansas 66047, United States

<sup>d</sup>Faculty of Pharmacy, The University of Manitoba, 750 McDermot Road, Winnipeg, Manitoba R3Y 2N2, Canada

### Abstract

TGX-221 is a potent, selective, and cell membrane permeable inhibitor of the PI3K p110 $\beta$  catalytic subunit. Recent studies showed that TGX-221 has anti-proliferative activity against PTEN-deficient tumor cell lines including prostate cancers. The objective of this study was to develop an encapsulation system for parenterally delivering TGX-221 to the target tissue through a prostate-specific membrane aptamer (PSMAa10) with little or no side effects. In this study, PEG-PCL micelles were formulated to encapsulate the drug, and a prodrug strategy was pursued to improve the stability of the carrier system. Fluorescence imaging studies demonstrated that the cellular uptake of both drug and nanoparticles were significantly improved by targeted micelles in a PSMA positive cell line. The area under the plasma concentration time curve of the micelle formulation in nude mice was 2.27-fold greater than the naked drug, and the drug clearance rate was 17.5-fold slower. These findings suggest a novel formulation approach for improving site-specific drug delivery of a molecular-targeted prostate cancer treatment.

### Keywords

PEG-PCL micelle; TGX-221; PSMA; target delivery

### Introduction

The phosphatidylinositol 3-kinase (PI3K)/ phosphatase and tensin homolog (PTEN)/Akt pathway is highly involved in different types of cancer.<sup>1</sup> PI3Ks are a family of enzymes that phosphorylate PI(4,5)P<sub>2</sub> (PIP<sub>2</sub>) to PI(3,4,5)P<sub>3</sub> (PIP<sub>3</sub>). PIP<sub>3</sub> is a lipid-signaling second messenger that further activates of its downstream effectors, such as Akt, PDK1 and Rac1/cdc42.<sup>2</sup> The activation of Akt simulates cell growth, proliferation and survival.<sup>3</sup> PTEN is a phosphatase that dephosphorylates PIP<sub>3</sub> back to PIP<sub>2</sub>.<sup>4</sup> The missing function of PTEN results in accumulation of PIP<sub>3</sub> that mimics the activation of PI3K and triggers cell growth.

\*Correspondence to: Dr. M. Laird Forrest, The University of Kansas, 2095 Constant Ave., Lawrence, KS 66047. mforrest@ku.edu. YZ and SD contributed equally to this study.

PTEN deficiency is found in many types of cancers, such as prostate cancer (LNCaP), brain cancer (U87MG) and breast cancer (BT549).<sup>5-7</sup>

There are three classes of PI3K isoforms. The most commonly studied class I PI3Ks are further divided into class IA and IB. Only class IA enzymes were clearly implicated in human cancers. Class IA PI3K consists of a p110 catalytic subunit and a regulatory subunit. There are three highly homologous p110 catalytic isoforms: p110alpha, p110beta and p110delta.<sup>8,9</sup> p110beta is a promising target in cancer therapy<sup>10,11</sup> and PTEN-deficient tumor cells mainly depend on p110beta for signaling and growth, not p110alpha.<sup>9</sup>

The synthetic small molecule TGX-221 (Figure 1) is a potent, selective and cell membrane permeable inhibitor of PI3K p110 beta catalytic subunit, which is critical for cell growth, proliferation and tumorigenesis of PTEN-deficient tumor cells including prostate cancers.<sup>12,13</sup> Therefore, PI3K p110 beta inhibitors have a great promise as novel chemotherapeutic agents to treat PTEN deficient cancer cells.<sup>13</sup> However, TGX-221 is poorly soluble and requires organic solvents, such as DMSO or propylene glycol, for intravenous injection, which may cause cardiac toxicity, unconsciousness, arrhythmia and cardiac arrest.<sup>14</sup>

The therapeutic index of anticancer drugs is often very narrow, and the cytotoxic dose of the drug in the desired tissues can be maintained over an extended period of time with minimal side effects by targeted delivery and controlled drug release.<sup>15,16</sup> Both passive and ligand-targeted nanoparticles have been developed for targeted delivery of cancer therapies.<sup>17,18</sup> Passively targeted nanoparticles can accumulate to a greater extent in tumors compared to healthy tissues due to the enhanced permeability and retention (EPR) effect. The high accumulation of nanoparticles in the tumor tissues is a consequence of the poorly aligned endothelial cells allowing nanoparticles to escape from the blood circulatory system and to pool in the tumor where there is a lack of effective lymphatic drainage.<sup>19,20</sup> Micelles are attractive nanoparticles for the delivery of hydrophobic drugs, since they form spontaneously in water after co-mixing the drug with an amphiphilic polymer. Both polyethylene glycol (PEG) and polycaprolactone (PCL) are FDA approved biocompatible and biodegradable materials. Micelles formed by PEG-PCL block copolymers have been used as an effective drug delivery system for lipophilic molecules.<sup>21-23</sup> Upon pooling in the tumor, micelles will slowly release the drug and then dissolve into non-toxic degradation products.<sup>24</sup> Nanoparticles actively targeted via ligand binding can target cancer cells that over express specific receptors or proteins.<sup>16</sup> The ligands, monoclonal antibodies or aptamers, can recognize and bind to complementary molecules expressed on the tumor cells. We hypothesized that the delivery of a TGX-221 analogue to prostate cancer cells may be improved if the drug is encapsulated in targeted-nanoparticles. The cancer-targeted nanoparticles should be effective in suppressing tumor growth and metastasis with reduced or lack of side effects associated with drug toxicities to normal tissues.

Aptamers are single- or double-stranded oligonucleotides that are modified to have high binding affinity and specificity to the targets,<sup>25</sup> and they have emerged as a novel class of active targeting moieties for therapeutic and diagnostic applications in cancer treatment. Prostate specific membrane antigen (PSMA) expression is confined primarily to prostate tissues.<sup>26,27</sup> The expression of PSMA in other tissues, such as the brain and small intestines, is approximately 1,000-fold less than that in the prostate.<sup>28</sup> Prostate specific membrane aptamer A10 (PSMAa10) has nM affinity to the membrane expressing PSMA, and it can be used to achieve specific targeting of the nanoparticles to prostate cancer cells.<sup>29</sup>

Due to the high biocompatibility of PEG-PCL block copolymers and the specific expression of PSMA on prostate cancer cells, the combination of PEG-PCL and PSMAa10 in a nanoparticle delivery system is promising for the targeted therapy of prostate cancer.

## Materials and Methods

### 1. Materials

Azide poly(ethylene glycol) (MW: 5,800) was purchased from Polymer Source Inc. (Quebec, Canada). Propargyl-dPEG®1-NHS ester was purchased from Quanta BioDesign Ltd. (Powell, Ohio). PSMAa10 {5'-[NH<sub>2</sub>-(CH<sub>2</sub>)<sub>6</sub>-PEG<sub>18</sub>-GGG AGG ACG AUG GGG AUC AGC CAU GUU UAC GUC ACU CCU UGU CAA UCC UCA UCG GC *inverted* T]-3', 2'F pyrimidines } was custom synthesized by Integrated DNA Technologies (Coralville, IA).  $\epsilon$ -caprolactone, IR-820, pyrene, 1-amino-3-butyne and 1-M HCl in diethyl-ether were purchased from Sigma-Aldrich Co. (St. Louis, MO). Resazurin blue, silica gel and the organic solvents were purchased from Fisher Scientific (Pittsburgh, PA).

### 2. TGX-221 and prodrug synthesis

All chemicals were used as received unless stated otherwise. NMR spectra were taken on a 400-MHz Bruker with the solvent peak as an internal reference. Mass spectra were run in the Electrospray Ionization Mass Spectrometry (ESI-MS) mode or Atmospheric Pressure Chemical Ionization Mass Spectrometry (APCI-MS) mode. Reactions that required an inert atmosphere were carried out under dry argon with flame-dried glassware. Tetrahydrofuran (THF) was freshly distilled over sodium-benzophenone. Dichloromethane (DCM), N, N-dimethylformaldehyde (DMF) and triethylamine (TEA) were freshly distilled over CaH<sub>2</sub>. The synthetic scheme of TGX-221 and its analog BL05 are shown in Scheme 1.

**Synthesis of compound 1**—Malonyl dichloride (3.2 mL, 32.0 mmol) was added dropwise to a solution of 2-amino-3-bromo-5-methylpyridine (5 g, 26.7 mmol) in dry DCM (50 mL) cooled to 0 °C. The mixture was stirred at ambient temperature (ca. 22 °C) for 48 h. The yellow precipitate was collected by filtration, washed with DCM (3 × 50mL), and dried under reduced pressure. The desired compound was obtained with a yield of 86 % (4.88 g), and identity was confirmed by <sup>1</sup>H-NMR. The crude compound was used in the next step without any further purification. The filtrate was concentrated by rotovaporation. The resulting residue was suspended in 100 mL of H<sub>2</sub>O, and the suspension was stirred at ambient temperature for 1 h. The suspension was filtered and the filtrate was neutralized with solid Na<sub>2</sub>CO<sub>3</sub> to recover the unreacted 2-amino-3-bromo-5-methylpyridine (0.84 g).

**Synthesis of compound 2**—Compound 1 (4.88 g, 19.13 mmol) was suspended in dry DCM (100 mL), and TEA (5.40 mL, 38.3 mmol) was added dropwise at 0 °C followed by methanesulfonyl chloride (MsCl) (2.90 mL, 26.8 mmol). The mixture was stirred at ambient temperature for 1 h. Morpholine (5.0 mL, 57.4 mmol) was added and the mixture was refluxed for 24 h. The solvent then was removed under reduced pressure, and the mixture was diluted with H<sub>2</sub>O to afford a pale yellow precipitate. The solid was collected by filtration, washed with 2 × 50 mL of H<sub>2</sub>O, and dried under reduced pressure. The residue was purified through a silica flash column using EtOAc: hexanes 3:1 as the eluting solvent. The desired compound was obtained as a yellow solid with a yield of 42 % (2.61 g).

**Synthesis of compound 3**—Compound 2 (2.53 g, 7.80 mmol) in dry DMF (50 mL) was mixed with N, N-diisopropylethylamine (4.0 mL), butyl vinyl ether (5.0 mL) and dichloro 1,1'-bis(diphenylphosphino)ferrocene palladium (II) (0.25 g, 0.20 mmol) at ambient temperature under argon for ca. 30 min until a homogeneous solution was formed. The solution then was heated to 120 °C and stirred for another 16 h. After the solution cooled, it

was poured into 200 mL of 1-M HCl at 0 °C. The mixture then was stirred at ambient temperature overnight and extracted with DCM (2 × 100 mL). The combined organic phases were washed with water and dried over Na<sub>2</sub>SO<sub>4</sub>. Removal of the solvent under reduced pressure followed by purification of the resulting residue through a silica flash column using EtOAc: hexanes 3:1 as the eluting solvent led to the desired compound with a yield of 60 % (1.35 g).

**Synthesis of compound 4**—Compound 3 (1.35 g, 4.69 mmol) in DCM and methanol (5 : 1, 84 mL) was combined with NaBH<sub>4</sub> (0.70 g, 18.5 mmol) in 5 portions at 0 °C. After 10 min, the cooling bath was removed and the mixture was stirred at ambient temperature for 3 h. Then the mixture was cooled to 0 °C and 20 mL of H<sub>2</sub>O was added slowly. The mixture was extracted with DCM (2 × 50 mL). The combined organic phases were washed with water (2 × 50 mL) and brine (30 mL) and then dried over Na<sub>2</sub>SO<sub>4</sub>. Removal of the solvent under reduced pressure followed by purification of the resulting residue through a silica flash column using EtOAc: hexanes 3:1 as the eluting solvent led to the desired compound with a yield of 86 % (1.17 g).

**Synthesis of compound 7**—A solution of compound 4 (1.17 g, 4.05 mmol) in 10 mL of dry DCM was cooled to 0 °C, and MsCl (1.70 mL, 24.3 mmol) was added dropwise followed by dry TEA (1.35 mL). After 10 min, the cooling bath was removed, and the reaction proceeded at ambient temperature for ca. 4 h until TLC showed that the starting material was consumed completely. The resulting mixture was washed with water (50 mL), 2-M aqueous NaOH (50 mL) and brine (50 mL), and then dried over Na<sub>2</sub>SO<sub>4</sub>. Removal of the solvent under reduced pressure followed by purification of the resulting residue through a silica flash column using EtOAc: hexanes 1:2 as the eluting solvent led to the desired compound as a pale yellow solid with a yield of 93 % (1.39 g).

**Synthesis of TGX-221(compound 5)**—A solution of compound 4 (0.70 g, 1.91 mmol) in 10 mL of dry DCM was cooled to 0 °C, and aniline (0.5 mL, 16.3 mmol) was added dropwise followed by dry TEA (1.0 mL). The mixture was refluxed for 4 h and then stirred at ambient temperature overnight. The mixture was washed with water (2 × 50 mL) and brine (50 mL), and then dried over Na<sub>2</sub>SO<sub>4</sub>. Removal of the solvent under reduced pressure followed by purification of the resulting residue through a silica flash column using EtOAc: hexanes 3:1 as the eluting solvent led to the desired compound as a pale yellow solid with a yield of 80 % (0.56 g).

**Synthesis of 2-(Phenylamino)ethanol (compound 6)**—We followed the procedure of Bhanu et al.<sup>30</sup> Briefly, a mixture of aniline (4.66 g, 50 mmol) and 2-bromoethanol (4.34 g, 33 mmol) was heated at 90 °C under an argon atmosphere for 4 h. The resulting solid was dissolved in ethyl acetate (100 mL), washed with 2-M aqueous NaOH (3x 20 mL) followed by brine (50 mL), and then dried over Na<sub>2</sub>SO<sub>4</sub>. Removal of the solvent under reduced pressure followed by purification of the resulting residue through a silica flash column using EtOAc: hexanes 1:2 as the eluting solvent led to the desired compound with a yield of 89 % (4.03 g).

**Synthesis of compound 8 (BL05)**—A solution of compound 5 (0.47 g, 1.28 mmol) in 10 mL of dry DCM was cooled to 0 °C, and a solution of 2-(phenylamino)ethanol (0.70 g, 5.12 mmol) in 5 mL of dry DCM was added dropwise followed by dry TEA (1 mL). After 10 min, the mixture was refluxed for ca. 15 h until TLC showed that the starting material was consumed completely. The resulting mixture was washed with 2-M aqueous HCl, water, saturated NaHCO<sub>3</sub> aqueous solution and brine, and then dried over Na<sub>2</sub>SO<sub>4</sub>. Removal of the solvent under reduced pressure followed by purification of the resulting residue through a

silica flash column using EtOAc: hexanes 5:1 as eluting solvent led to the desired compound with a yield of 69 % (0.36 g).

**Synthesis of BL05-palmitate derivative (BL05-PA)**—BL05 (compound 8) (0.10 g, 0.24 mmol) and palmitic anhydride (0.24 g, 0.48 mmol) were suspended in 10 mL of dry DCM, and 0.20 mL of dry pyridine was added dropwise. The mixture was stirred overnight at ambient temperature until TLC showed that the starting material was consumed completely. The resulting mixture was washed with 2-M aqueous HCl (30 mL), water, saturated NaHCO<sub>3</sub> aqueous solution and brine. Removal of the solvent under reduced pressure followed by purification of the resulting residue through a silica flash column using EtOAc: hexanes 3:1 as the eluting solvent led to the desired compound with a yield of 95 % (0.15 g).

**Synthesis of BL05-hexanoate derivative (BL05-HA)**—A solution of BL05 (compound 8) (0.18 mg, 0.45 mmol) in 5 mL of dry DCM was cooled to 0 °C, and hexanoyl chloride (0.26 mL, 1.80 mmol) was added followed by dry pyridine (0.38 mL). After 10 min, the cooling bath was removed, and the reaction proceeded at ambient temperature overnight until TLC showed that the starting material was consumed completely. The resulting mixture was washed with 2-M aqueous HCl, water, saturated NaHCO<sub>3</sub> aqueous solution and brine. The organic phase was dried over Na<sub>2</sub>SO<sub>4</sub>. Removal of the solvent under reduced pressure followed by purification of the resulting residue through a silica flash column using EtOAc: hexanes 2:1 as the eluting solvent led to the desired compound as a pale yellow solid with a yield of 91 % (0.266 g).

### 3. Synthesis of Azide Poly(ethylene glycol)-block-Poly( $\epsilon$ -caprolactone) Copolymers (N<sub>3</sub>-PEG-PCL)

All glassware were flamed dried under vacuum and were handled under a dry argon stream. The N<sub>3</sub>-PEG-PCL copolymer was prepared by acid catalyzed ring-opening polymerization reaction of  $\epsilon$ -caprolactone in the presence of N<sub>3</sub>-PEG-OH as an initiator. The typical process is described as follows. N<sub>3</sub>-PEG-OH was azeotropically dried using anhydrous toluene under reduced pressure.  $\epsilon$ -caprolactone was dried over CaH<sub>2</sub> overnight and then distilled under vacuum. N<sub>3</sub>-PEG-OH (0.375 g, 0.0647 mmol) was dissolved in 8 mL of dry DCM, followed by the addition of 0.75 mL of  $\epsilon$ -caprolactone (100 eq). The polymerization was initiated by the addition of 1-M HCl in diethyl ether (0.8 mL, 3 eq) at 25 °C. After 24 h, the mixture was poured into diethyl ether to precipitate the copolymer. Then, the N<sub>3</sub>-PEG-PCL copolymer was further purified by precipitation in cold acetone. The residual solvent was removed under reduced pressure.

### 4. Characterization of the polymeric material

The N<sub>3</sub>-PEG-PCL was dissolved in CDCl<sub>3</sub> for <sup>1</sup>H-NMR spectroscopy. Gel permeation chromatography (GPC) was used to determine the polymer molecular weight distribution. GPC analysis was performed on a Shodex GPC LF-804 column thermostated at 40°C with DMF and 10-mM LiCl as the mobile phase at a flow rate of 0.8 mL/min. Peaks were detected using a refractive index detector (RID-10A, Shimadzu). Narrow molecular weight distribution polyethylene glycols (Scientific Polymer Products Inc., Ontario, NY) were used as standards for GPC analysis.

### 5. Micelle preparation

The N<sub>3</sub>-PEG-PCL (15 mg, 1.3 mmol) was dissolved in 0.5 mL of dimethylacetamide (DMAc) and the organic solution was added dropwise to 2 mL of ddH<sub>2</sub>O with mechanical stirring. The organic solvent was removed by overnight dialysis against phosphate buffered

saline (PBS) using 10-kDa molecular weight cutoff (MWCO) dialysis tubing (Spectrum Laboratories, Rancho Dominguez, CA). Drug-loaded micelles were prepared by mixing the drugs with the copolymer in DMAc before adding ddH<sub>2</sub>O.

The aptamer, PSMAa10, was functionalized by addition of an alkyne group using the following procedure. PSMAa10 (0.2  $\mu$ mol, 3.7 mg) was dissolved in 500  $\mu$ l of 0.1-M carbonate buffer (pH 9.0). The alkyne-NHS ester (2.3 mg) was dissolved in 60  $\mu$ l of DMSO, and 6  $\mu$ l of the alkyne-modified NHS ester solution was added to the carbonate buffer containing the aptamer. After mixing for 4 h at ambient temperature, the alkyne modified PSMAa10 was purified using a centrifugal filtration device (Amicon<sup>®</sup> Ultra Centrifugal Filter 10K, Millipore Corp.).

The near infrared dye, IR-820, was modified to include an alkyne by conjugation of 1-amino-3-butyne. Briefly, 150 mg of IR-820 (0.177 mmol) was dissolved in 10 mL of DMF. Then, 61 mg of 1-amino-3-butyne (5 eq) and 123  $\mu$ l of TEA (5 eq) were added. The solution was stirred at 40 °C for 8 h. The final product was purified by silica flash chromatography using EtOAc: methanol 1:2 as the elution solvent.

Both alkyne modified PSMAa10 and IR-820 were conjugated to the micelle's surface by azide alkyne Huisgen cycloaddition (i.e. click reaction). Briefly, 50  $\mu$ g of alkyne modified PSMAa10 and 100  $\mu$ g of alkyne modified IR-820 were added to N<sub>3</sub>-PEG-PCL micelles (2.5 mg/mL) prepared in ddH<sub>2</sub>O. Copper sulfate (0.6  $\mu$ mol/mL) and sodium ascorbate (3.0  $\mu$ mol/mL) were used as a catalyst. The reaction mixture was gently stirred at ambient temperature overnight. The modified micelles were purified by dialysis against PBS using 10,000 MWCO dialysis tubing (SnakeSkin<sup>®</sup> Pleated Dialysis Tubing, Thermo Scientific) for 24 h. To determine the extent of the reaction, the supernatant was separated from the micelle solution using a Microcon YM-100 centrifugal concentrator (0.5-mL capacity, NMWL 100, 000, Millipore Corp.) at 11,000 $\times$ g for 15 min. The filtrate was analyzed by high-performance liquid chromatography (HPLC) (LC-2010CHT, Shimadzu).

## 6. Micelle characterization

The critical micelle concentration (CMC) of N<sub>3</sub>-PEG-PCL micelles was determined by measuring the excitation ratio of pyrene using a fluorophotometer (RF-5301 PC, Shimadzu). For example, solutions of N<sub>3</sub>-PEG-PCL micelles were prepared by serial dilution and then incubated with 0.6- $\mu$ M pyrene for 1 h at 65 °C and then 18 h at ambient temperature in the dark. The fluorescent emission of pyrene was measured at 390 nm. The fluorescent excitation ratio of pyrene at 339 and 334 nm changes in response to the probe's microenvironment polarity. A sharp increase in the 339/334 excitation ratio indicates the CMC as the pyrene preferentially partitions into the hydrophobic core of N<sub>3</sub>-PEG-PCL micelles.

The formation of micelles was determined by GPC (Shodex OHpak SB-803 HQ, Showa Denko America, Inc.) using a Shimadzu 2010CHT system. GPC was performed using ddH<sub>2</sub>O as the mobile phase with a flow rate of 0.8 mL/min, and the GPC column was thermostated at 40 °C. Elution peaks were detected using an evaporative light scattering detector (ELSD-LTII, Shimadzu). The size and polydispersity of micelles were measured with a ZetaPALS (Brookhaven Instruments Corp.) using the Gaussian distribution.

The drug loading efficiency (DL %) and encapsulation efficiency (EE %) of BL05-HA in PEG-PCL micelles were calculated according to the following equations:

$$DL\% = \frac{\text{weight of the drug in micelle}}{\text{weight of the polymer and drug}} \times 100\%$$
$$EE\% = \frac{\text{weight of the drug in micelle}}{\text{weight of the feeding drug}} \times 100\%$$

GPC micelle fraction was collected and dried by speed-vap. The dried micelle fraction was weighed to determine weight of the polymer and drug. Then, the dried micelle was redissolved in MeOH and drug weight in micelle was evaluated by HPLC analysis.

## 7. Cytotoxicity assay

The prostate cancer cell lines DU145 and LNCaP were maintained in RPMI-1640 medium, and PC3 cells were maintained in F-12K medium (ATCC, Manassas, VA). LNCaP is a PSMA positive cell line, whereas DU145 and PC3 are PSMA negative. Both were supplemented with 10 % fetal bovine serum (Hyclone Laboratory Inc., Logan, Utah). Cells were plated in 96-well flat-bottomed plates at a concentration of 5,000 cells per well in 90  $\mu$ l of growth medium. After 12 h, TGX-221, BL05, or BL05-HA loaded micelles in PBS were added at concentrations of 0, 0.1, 1, 5, 10, 50 or 100  $\mu$ M. PBS and 10  $\mu$ l of trichloroacetic acid (TCA) were added to negative and positive control wells, respectively. After 72 h, 10  $\mu$ l of 55- $\mu$ M resazurin blue was added to each well and incubated at 37  $^{\circ}$ C for 4 h. After incubation, the resorufin product was measured with a fluorophotometer (SpectraMax Gemini; Molecular Devices, CA) using an excitation wavelength of 560 nm and an emission wavelength of 590 nm. The IC<sub>50</sub> was determined as the midpoint between positive and negative control groups for each plate using GraphPad Prism 5 software (GraphPad Software Inc., San Diego, CA).

## 8. Western blot assay

After serum starvation for 16 h, LNCaP cells were treated with 2- $\mu$ M TGX-221 or BL05 and 100-ng/mL EGF for 30 min. Then, cells were pelleted and lysed with cell lysis buffer containing protease inhibitors. Protein concentrations were determined by BCA assays, and equal amounts of protein extract were separated on a 10 % SDS-polyacrylamide gel, transferred to a nitrocellulose membrane and immunoblotted with anti-pAkt (Ser-473) and Akt (Cell Signaling Technology, Inc., Danvers, MA) followed HRP-conjugated secondary antibodies (Santa Cruz Biotech, Inc., Santa Cruz, CA). The specific bands were detected using a chemiluminescence luminal reagent (Santa Cruz Biotech, Inc., Santa Cruz, CA).

## 9. In vitro drug release study

The in vitro release of the drug from N<sub>3</sub>-PEG-PCL micelles into PBS (pH 7.4) was monitored by a dialysis method.<sup>31</sup> Dialysis was carried out at 37  $^{\circ}$ C under sink condition using 10-kDa MWCO dialysis tubing (SnakeSkin<sup>®</sup>, Thermo Scientific Inc., Rockford, IL). The initial volume of drug-loaded micelles in the dialysis tubing was 5 mL and the sink solution was 4 L. The PBS was changed several times per day to maintain sink conditions. After pre-determined time intervals, samples were withdrawn from the dialysis tubing and analyzed by HPLC with a reversed phase column (TSK-GEL<sup>®</sup> ODS-100Z, Tosoh Bioscience) at 50  $^{\circ}$ C with UV detection at 280 nm. The chromatography conditions were a mobile phase A of 100 % ddH<sub>2</sub>O and B of 100 % methanol at a flow rate of 1 mL/min. The gradient program was i) a linear gradient from 50 % to 90 % solvent B over 5 min; ii) 3.5 min with 90 % solvent B; iii) 6.5 min with 100% solvent B; and iv) 10 min with 50% solvent B. Retention times: TGX-221 6.86 min; BL05 6.93 min; BL05-HA 10.14 min and BL05-PA 17.04 min.

## 10. Uptake of PSMA-targeted micelles by prostate cancer cells

Fluorescence microscopy was used to examine cellular uptake of IR-820-labeled PSMA-targeted micelles. PSMA negative PC3 cells and PSMA positive LNCaP cells were seeded at a density of  $1 \times 10^6$  cells in an 8.6-cm<sup>2</sup> chamber slide system (Thermo Scientific). After cells had attached to the microscope slide's surface, the PC3 and LNCaP cells were incubated with the PSMA-targeted (2.5 % weight compared with polymer concentration) or non-targeted micelles for 6 h at 37 °C. Unbound micelles were removed by washing 3 times with PBS. Fluorescence images were acquired using a Cy5 filter set on a Nikon Eclipse 80i microscope equipped for epifluorescence and an Orca ER camera (Hamamatsu Inc., Bridgewater, NJ).

The cellular uptake and accumulation of PSMA targeted micelles (2.5 % weight compared with polymer concentration) was quantified in LNCaP and PC3 cells. Cells were seeded in 96-well flat-bottom plates at a concentration of 5,000 cells per well in 90  $\mu$ l of growth medium. After the cells attached to the surface, 10  $\mu$ l of targeted or non-targeted IR-820-modified micelles were added at different concentrations. After 6 h of incubation, the growth medium was removed and each well was washed with PBS. The plate fluorescence was measured using a fluorophotometer at an excitation wavelength of 675 nm and an emission wavelength of 750 nm.

## 11. Pharmacokinetic evaluation

Male Balb/c mice were maintained in a temperature-controlled room with a 12 h light/dark cycle for at least one week prior to the study. The animal protocol was approved by the Institutional Animal Care and Use Committee (IACUC) at the University of Kansas Medical Center. Animals were administered BL05-HA loaded PSMA-targeted micelles or BL05-HA prepared in propylene glycol at a dose of 30 mg/kg via tail vein injection (100  $\mu$ l). Blood samples were withdrawn after 5 min, 1, 2, 4, 6, 12 and 24 h from the saphenous vein. A 20- $\mu$ l blood sample was added to 50  $\mu$ l of Alsever's solution, which is an anticoagulant. After gently mixing, the blood sample was centrifuged at 3,000 rpm for 10 min. Plasma was prepared by solid phase extraction (SPE) prior to the HPLC analysis. Briefly, plasma sample diluted with 2% NH<sub>4</sub>OH (1:3) was applied to the SPE column (Bond Elut-C18, Agilent Technologies, Lake Forest, CA) that was pretreated with 100% MeOH and equilibrated with 100 % ddH<sub>2</sub>O. Sample was washed with 5% MeOH in ddH<sub>2</sub>O and eluted twice with 150  $\mu$ l 100 % MeOH.

## 12. Statistical analysis

GraphPad Prism 5 software was used for statistical analysis. A *t*-test was used to test for differences between two data sets, while a one-way ANOVA and Tukey post test was used to analyze the differences when more than two data sets were compared. In all comparisons, statistical significance was set at *p* < 0.05.

## Results

### 1. Drug synthesis

We successfully synthesized TGX-221, BL05 and the fatty acid prodrugs. The synthesis of TGX-221 was accomplished with 2-amino-3-bromo-5-methylpyridine and malonyl dichloride as the starting materials through 6 steps with an overall yield of 14 % and BL05 with an overall yield of 12 %. The structure of each compound was determined by <sup>1</sup>H-NMR, <sup>13</sup>C-NMR or together with high resolution APCI-MS or ESI-MS.



**Compound 1**—<sup>1</sup>H-NMR (DMSO-*d*<sub>6</sub>, 400 MHz): δ = 8.74 (s, 1H), 8.29 (s, 1H), 5.55 (s, 1H), 2.34 (s, 3H), which was consistent with the reported data.

**Compound 2**—<sup>1</sup>H-NMR (CDCl<sub>3</sub>, 400 MHz): δ = 8.72 (s, 1H), 7.87 (d, *J* = 1.9 Hz, 1H), 5.61 (s, 1H), 3.84-3.80 (m, 4H), 3.74-3.69 (m, 4H), 2.35 (s, 3H), which was consistent with the reported data.

**Compound 3**—<sup>1</sup>H-NMR (CDCl<sub>3</sub>, 400 MHz): δ = 8.88 (s, 1H), 7.86 (d, *J* = 2.2 Hz, 1H), 5.66 (s, 1H), 3.84-3.79 (m, 4H), 3.67-3.62 (m, 4H), 2.79 (s, 3H), 2.38 (d, *J* = 1.0 Hz, 3H), which was consistent with the reported data.

**Compound 4**—<sup>1</sup>H-NMR (CDCl<sub>3</sub>, 400 MHz): δ = 8.67 (s, 1H), 7.50 (d, *J* = 1.9 Hz, 1H), 5.63 (s, 1H), 5.25-5.18 (m, 1H), 4.63 (d, *J* = 5.0 Hz, 1H), 3.82 (t, *J* = 2.9 Hz, 4H), 3.61 (t, *J* = 4.2 Hz, 4H), 2.35 (d, *J* = 1.0 Hz, 3H), 1.63 (d, *J* = 6.6 Hz, 3H); <sup>13</sup>C-NMR (CDCl<sub>3</sub>, 100 MHz): δ = 18.1, 22.1, 44.5 (x2), 49.1, 66.4 (x2), 81.1, 117.4, 122.3, 135.3, 137.3, 147.5, 159.0, 160.2; HRMS (ESI) Calc'd for C<sub>15</sub>H<sub>19</sub>N<sub>3</sub> NaO<sub>3</sub> (M + Na)<sup>+</sup> : 312.1324; Found: 312.1329.

**Compound 5 (TGX-221)**—<sup>1</sup>H-NMR (CDCl<sub>3</sub>, 400 MHz): δ = 8.67 (s, 1H), 7.60 (d, *J* = 2.0 Hz, 1H), 7.13 (d, *J* = 7.4 Hz, 1H), 7.12 (d, *J* = 6.6 Hz, 1H), 6.68 (t, *J* = 7.3 Hz, 1H), 6.48 (d, *J* = 7.6 Hz, 2H), 5.68 (s, 1H), 5.15 (d, *J* = 5.6 Hz, 1H), 4.39 (bs, 1H), 3.81 (t, *J* = 5.0 Hz, 4H), 3.72-3.62 (m, 4H), 2.26 (d, *J* = 1.0 Hz, 3H), 1.59 (d, *J* = 6.8 Hz, 3H); <sup>13</sup>C-NMR (CDCl<sub>3</sub>, 100 MHz): δ = 18.3, 22.1, 44.6 (x2), 49.1, 66.6 (x2), 81.3, 113.2 (x2), 117.6, 122.5, 123.8, 129.2 (x2), 135.4, 137.3, 146.8, 147.5, 159.1, 160.2; HRMS (ESI) Calc'd for C<sub>21</sub>H<sub>25</sub>N<sub>4</sub>O<sub>2</sub> (M + H)<sup>+</sup> : 365.1978; Found: 365.1975.

**Compound 6**—<sup>1</sup>H-NMR (CDCl<sub>3</sub>, 400 MHz): δ = 7.22 (dd, *J* = 7.4, 7.3 Hz, 2H), 6.78 (d, *J* = 7.3 Hz, 1H), 6.69 (d, *J* = 7.7 Hz, 2H), 3.84 (t, *J* = 5.1 Hz, 2H), 3.32 (t, *J* = 4.9 Hz, 2H), 3.03 (bs, 2H).

**Compound 7**—<sup>1</sup>H-NMR (CDCl<sub>3</sub>, 400 MHz): δ = 8.89 (dd, *J* = 2.1, 1.1 Hz, 1H), 7.87 (d, *J* = 2.2 Hz, 1H), 5.88 (q, *J* = 6.8 Hz, 1H), 5.68 (s, 1H), 3.82 (t, *J* = 5.2 Hz, 4H), 3.65 (t, *J* = 5.1 Hz, 4H), 3.16 (s, 3H), 2.39 (d, *J* = 0.9 Hz, 3H), 1.88 (d, *J* = 6.8 Hz, 3H); HRMS (ESI) Calc'd for C<sub>16</sub>H<sub>22</sub>N<sub>3</sub>O<sub>5</sub> S (M + H)<sup>+</sup> : 368.1280; Found: 368.1276.

**Compound 8 (BL05)**—<sup>1</sup>H-NMR (CDCl<sub>3</sub>, 400 MHz): δ = 8.70 (s, 1H), 7.45 (s, 1H), 7.22 (d, *J* = 8.6 Hz, 1H), 7.20 (d, *J* = 8.5 Hz, 1H), 6.86 (d, *J* = 8.2 Hz, 2H), 6.76 (t, *J* = 6.9 Hz, 1H), 5.64-5.60 (m, 1H), 5.59 (s, 1H), 3.63-3.57 (m, 4H), 3.54 (t, *J* = 6.0 Hz, 2H), 3.44 (t, *J* = 5.6 Hz, 2H), 3.41-3.35 (m, 4H), 2.34 (s, 3H), 1.62 (d, *J* = 7.0 Hz, 3H); <sup>13</sup>C-NMR (CDCl<sub>3</sub>, 100 MHz): δ = 16.9, 18.4, 44.4 (x2), 47.3, 52.3, 60.0, 66.5 (x2), 81.3, 114.2 (x2), 117.8, 121.7, 124.3, 129.2 (x2), 135.5, 136.5, 148.0, 148.2, 159.0, 160.1; HRMS (ESI) Calc'd for C<sub>23</sub>H<sub>29</sub>N<sub>4</sub>O<sub>3</sub> (M + H)<sup>+</sup> : 409.2240; Found: 409.2229.

**BL05-PA**—<sup>1</sup>H-NMR (CDCl<sub>3</sub>, 400 MHz): δ = 8.71 (s, 1H), 7.42 (d, *J* = 1.8 Hz, 1H), 7.23 (d, *J* = 8.7 Hz, 1H), 7.21 (d, *J* = 8.7 Hz, 1H), 6.81 (d, *J* = 8.2 Hz, 2H), 6.74 (t, *J* = 7.2 Hz, 1H), 5.61 (s, 1H), 5.60-5.57 (m, 1H), 4.16-4.09 (m, 1H), 4.00-3.93 (m, 1H), 3.67-3.59 (m, 5H), 3.58-3.49 (m, 1H), 3.41 (t, *J* = 4.9 Hz, 4H), 2.34 (d, *J* = 0.9 Hz, 3H), 2.28 (t, *J* = 7.5 Hz, 2H), 1.66 (d, *J* = 7.2 Hz, 4H), 1.61 (t, *J* = 7.2 Hz, 2H), 1.35-1.22 (bs, 23H), 0.90 (t, *J* = 7.0 Hz, 3H); <sup>13</sup>C-NMR (CDCl<sub>3</sub>, 100 MHz): δ = 14.1, 17.5, 18.4, 22.7, 24.9, 29.2, 29.3, 29.4 (x2), 29.5 (x2), 29.6 (x2), 29.7 (x2), 31.9, 34.2, 44.0, 44.4 (x2), 51.8, 61.8, 66.5 (x2), 81.3, 113.1 (x2), 117.4, 121.7, 124.2, 129.3 (x2), 135.7, 136.0, 147.7, 147.9, 159.0, 160.1, 173.7; HRMS (ESI) Calc'd for C<sub>39</sub>H<sub>59</sub>N<sub>4</sub>O<sub>4</sub> (M+H)<sup>+</sup> : 647.4536; Found: 647.4528.

**BL05-HA**— $^1\text{H-NMR}$  ( $\text{CDCl}_3$ , 400 MHz):  $\delta$  = 8.71 (s, 1H), 7.42 (d,  $J$  = 1.8 Hz, 1H), 7.23 (d,  $J$  = 8.8 Hz, 1H), 7.22 (d,  $J$  = 8.7 Hz, 1H), 7.21 (d,  $J$  = 8.7 Hz, 1H), 6.81 (d,  $J$  = 8.2 Hz, 2H), 6.74 (t,  $J$  = 7.2 Hz, 1H), 5.61 (s, 1H), 5.60-5.57 (m, 1H), 4.17-4.09 (m, 1H), 4.00-3.93 (m, 1H), 3.70-3.58 (m, 5H), 3.41 (t,  $J$  = 4.9 Hz, 4H), 2.34 (d,  $J$  = 0.9 Hz, 3H), 2.28 (t,  $J$  = 7.4 Hz, 2H), 1.66 (d,  $J$  = 7.0 Hz, 3H), 1.64-1.58 (m, 1H), 1.38-1.26 (m, 5H), 0.91 (t,  $J$  = 6.8 Hz, 3H);  $^{13}\text{C-NMR}$  ( $\text{CDCl}_3$ , 100 MHz):  $\delta$  = 13.9, 17.4, 18.4, 22.3, 24.6, 31.3, 34.1, 44.0, 44.4 (x2), 51.8, 61.8, 66.5 (x2), 81.3, 113.1 (x2), 117.4, 121.7, 124.2, 129.3 (x2), 135.7, 136.0, 147.7, 147.9, 159.0, 160.1, 173.7; HRMS (ESI) Calc'd for  $\text{C}_{29}\text{H}_{39}\text{N}_4\text{O}_4$  ( $\text{M} + \text{H}$ ) $^+$  : 507.2971; Found: 507.2955.

## 2. PEG-PCL micelle preparation and characterization

The  $\text{N}_3$ -PEG-PCL block copolymer was synthesized by a ring opening reaction.  $^1\text{H-NMR}$  spectra showed two main peaks at 3.67 (-OCH<sub>2</sub>CH<sub>2</sub>) and 4.08 (-OCH<sub>2</sub>CH<sub>2</sub>CH<sub>2</sub>CH<sub>2</sub>CH<sub>2</sub>CO-) that correspond to PEG and PCL, respectively. The molecular weight of  $\text{N}_3$ -PEG-PCL copolymer determined by  $^1\text{H-NMR}$  was 5,800:5,800 and the polydispersity of this polymer measured by GPC was 1.10. The CMC was determined to be 300 nM using the pyrene incorporation assay. Based on Gibb's free energy of micellization, the nanomolar CMC of PEG-PCL copolymer indicated that the micelle had high thermodynamic stability. For 10 % (w/w) BL05-HA loaded PEG-PCL micelles, DL % was  $9.5 \pm 0.2$  % and EE % was  $74.5 \pm 4.6$  %.

The  $\text{N}_3$ -PEG-PCL micelles were prepared using a solvent displacement method. The PCL block served as a hydrophobic core of the micelle and physically entrapped the poorly water soluble anticancer drug into the micelle. GPC was used to confirm the formation of PEG-PCL micelles. PEG-PCL micelles are known to be stable when diluted below the CMC during GPC analysis, which reflects a high kinetic stability against dissociation.<sup>32</sup> The micelles' hydrodynamic diameter from DLS with Gaussian volume weighting was approximately 50 nm (Table 1), which is suitable for intravenous administration and extravasation in tumors.<sup>33</sup>

## 3. Conjugation of PSMAa10 to PEG-PCL micelles

The alkyne modified aptamer, PSMAa10, was confirmed by ESI-MS ( $[\text{M}+\text{Na}]^+ = 18,928.0$ ). The alkyne modified PSMAa10, was conjugated to the azide end group of the PEG-PCL copolymer by the Huisgen cycloaddition click reaction. The conjugation efficiency was determined by quantifying the unconjugated ligand remaining in the supernatant. The amount of PSMAa10 conjugated to the  $\text{N}_3$ -PEG-PCL micelle surface increased with increasing reaction time: 1 h,  $0.017 \pm 0.005$  (yield: 14.2 %); 3 h,  $0.103 \pm 0.010$  (yield: 20.6%); 5 h,  $0.123 \pm 0.015$  (yield: 24.6 %) mg PSMAa10 / mg  $\text{N}_3$ -PEG-PCL. Since precipitation occurred after 5-h, the Click reaction time was controlled at 3 h. The conjugation of PSMAa10 to the micelle's surface was examined by agarose gel electrophoresis (data not shown). The near infrared fluorophore IR-820 was functionalized with an alkyne by TEA buffered condensation with 1-amino-3-butyne. The successful conjugation was confirmed by ESI-MS. The micelle surface also was modified with IR-820 by click reaction. The IR-820 conjugated micelles had a maximum absorption wavelength of 675 nm and an emission wavelength of 745 nm.

## 4. Characterization of conjugated PEG-PCL micelles

Particle sizes of different micelle formulations were determined by dynamic light scattering (Table 1). The sizes of all of the nanoparticle formulations were smaller than 100 nm, which is suitable for intravenous application. The in vitro release half-lives of TGX-221, BL05, BL05-HA and BL05-PA were investigated at simulated in vivo conditions using a bath at pH 7.4 and 37 °C (Table 1). In addition, the release half-lives of TGX-221 and its analog,

BL05, from PEG-PCL micelles were identical, which is likely due to the similar lipophilicity of the two compounds. TGX-221 had a calculated  $\log P_{o/w}$  of  $2.14 \pm 0.68$  and BL05 was  $1.81 \pm 0.67$  (ALogPS 2.1, <http://www.vcclab.org>). The more hydrophobic ester prodrugs, BL05-HA ( $\log P_{o/w}$   $4.15 \pm 0.31$ ) and BL05-PA ( $\log P_{o/w}$   $8.42 \pm 0.83$ ), had much longer release half-lives of 5 and 6.5 days in PEG-PCL micelles, respectively. The prodrugs tended to stay in the hydrophobic PCL core of the micelle, and they were protected from hydrolysis in the hydrophobic core due to limited penetration of water. The aptamer conjugated micelle was larger than the non-targeted micelle, and the conjugation of IR-820 was confirmed by observing the increased Stokes shift of fluorescent dye. The Stokes shift of IR-820 increased after conjugation to the micelle surface due to electromagnetic retardation<sup>34</sup>.

## 5. In vitro cytotoxicity studies

The  $IC_{50}$ s of TGX-221, BL05 and BL05-HA were determined in DU145, PC3 and LNCaP cells (Table 2). BL05-PA was not soluble in PBS with 1 % DMSO, and it was not tested further. TGX-221, BL05 and BL05-HA showed selective cytotoxicity to LNCaP cells, which may be due to the deficiency of PTEN in this cell line and the accumulation of PIP3 in the cells. A Western blot was performed to determine if both TGX-221 and BL05 are involved in the same cell signaling pathway that contributes to the selective cytotoxicity. As demonstrated by Western blot, TGX-221 and BL05 inhibited phosphorylation of Akt (Figure 2), which in turn indicated the inhibitor of PI3K activity.

The cytotoxicity of empty micelles, PSMA-targeted empty micelles, IR-820-labeled empty micelles and IR-820-labeled PSMA-targeted micelles was examined in DU145 prostate cancer cells (Figure 3). The drug free targeted micelles did not inhibit cell growth. However, the dye-labeled micelles did inhibit cell growth, so they were not characterized further in vivo.

## 6. Micelle formulation effects on cellular uptake of the drug

The DU145 cells were treated with BL05-HA in DMSO and BL05-HA loaded in non-targeted micelles. The solubility of BL05-HA in 5 % DMSO was determined to be  $32.35 \mu\text{g/ml}$  ( $49.86 \mu\text{M}$ ). After a 12-h treatment, the cell culture medium was analyzed for extracellular drug content by HPLC, and the drug uptaken by the cells was quantified (Figure 4). Micelle formulations significantly improved the cellular uptake at all concentrations, also DMSO was not required to solubilize BL05-HA in the micelle formulation.

## 7. PSMAa10 targeting improved cellular uptake of both micelles and drug by PSMA-positive cells

LNCaP cells (PSMA +) were treated with PSMA-targeted and IR-820-labeled micelles with increasing substitutions of the aptamer. The micelle uptake was estimated by the relative fluorescence intensity of the IR-820. The fluorescence increased with increasing aptamer substitution: 1 %,  $325 \pm 103.410$ ; 2.5 %,  $574.554 \pm 33.614$ ; 5 %,  $704.055 \pm 73.235$  and 10 %,  $945.311 \pm 145.445$  RFU.

Confocal microscopy was used to examine if PSMA targeting can improve the micelle uptake by PSMA presenting cells. The aptamer did not improve the micelle uptake in the PSMA-negative PC3 cells. However, in the PSMA-positive LNCaP cells, we detected more fluorescence signal in cells treated with PSMA-targeted micelles (Figure 5). The uptake was then quantified with a fluorescence plate reader. The fluorescence signal was significantly higher in PSMA-positive cells (LNCaP) treated with PSMA-targeted micelles. However, in

PSMA-negative PC3 cells, the fluorescence was not enhanced by addition of PSMA to the micelles (Figure 6).

The effect of PSMA-targeting of micelles on the cellular uptake of BL05-HA was examined in both DU145 (PSMA -) and LNCaP (PSMA +) cells (Figure 7). PSMA-targeted micelles significantly improved the drug uptake in PSMA-positive LNCaP cells but not PSMA-negative DU145. In addition, BL05-HA formulated in PSMA-targeted micelles significantly reduced LNCaP cell viability compared to the naked drug, whereas BL05-HA in non-targeted micelles was no more effective than the naked drug. In PSMA negative cells, this significant effect was not observed (Figure 8) ( $p > 0.05$ ).

## 8. Pharmacokinetic evaluation

The pharmacokinetics of naked BL05-HA and BL05-HA formulated in PSMA-targeted micelles were compared in male Balb/c mice ( $n = 3$ ). The initial drug plasma concentration ( $C_0$ ) of the micelle formulation was 1.42-fold greater than the naked drug (Figure 9). The plasma concentration of BL05 delivered by PSMA-targeted micelles was higher than the naked drug at all time points. A two-compartment pharmacokinetic model was selected to describe the biexponential nature of the pharmacokinetics disposition of PEG-PCL micelle formulation, whereas one-compartment model was used in BL05-HA naked drug and the related pharmacokinetic parameters are listed in Table 3. The area under the plasma concentration time curve ( $AUC_{0-24h}$ ) of the micelle formulation was 2.27-fold greater than that of the naked drug and the concomitant total body clearance was 17.5-fold lower.

## Discussion

Prostate cancer is by far the most commonly diagnosed cancer among Western Males. Most anticancer drugs are administered intravenously or orally to achieve systemic distribution, and the non-specific uptake of anticancer drugs may cause damage to healthy rapidly dividing cells, such as bone marrow and hair.<sup>35, 36</sup> Nanoparticles can passively or actively target to tumor tissue and minimize the side effects of conventional chemotherapies, such as sexual dysfunction, cardiac toxicity, gastrointestinal damage, and neurotoxicity.<sup>37</sup> The leaky endothelial vasculature of tumor tissues and the size properties of nanoparticles play a significant role in passive targeting,<sup>38</sup> due to the EPR effect. Improved targeting can be achieved by decorating the nanoparticle surface with a tumor specific targeting molecule, such as a monoclonal antibody or nucleic acid.<sup>39</sup> The tumor specific targeting molecules can bind to tumor cells and increase the intracellular concentration of the drug by receptor-mediated endocytosis. In this study, we formulated a prostate cancer cell-targeted nanocarrier that can enhance the efficacy of an encapsulated anticancer drug against prostate cancer cells and also optimize the pharmacokinetic disposition of the drug in a mouse model because of the encapsulated carrier. We targeted the carriers to prostate cells with the PSMA aptamer, because this small ligand has nM affinities for the PSMA receptor, which is ubiquitous to clinical prostate cancers.<sup>40</sup> We conjugated the ligand to pre-formed micelles. This approach is expected to result in a more homogenous distribution of the ligands among the nanoparticles than other approaches, such as attaching ligands to the monomers before formation or drug encapsulation. The resulting triazole linker also is more resistant to hydrolytic and enzymatic cleavage than esters or amides formed by carbodiimide chemistries.

TGX-221 showed selective cytotoxicity against LNCaP cells, which was consistent with a previous report.<sup>13</sup> TGX-221 and its analog, BL05, showed similar toxicity in different prostate cancer cell lines, and Western blotting confirmed their inhibitory effects on phosphorylation of Akt in LNCaP cells. The modification of the aniline nitrogen did not

affect the drug activity significantly, which is possible if only the morpholinechromone ring system and aniline structure contribute to the binding to PI3K beta subunit.<sup>41</sup>

Drug interaction and association with the hydrophobic core of the micelle can influence a drug's release rate.<sup>42</sup> Both TGX-221 and BL05 did not stay in the hydrophobic core of PEG-PCL micelles, which may be due to the amphiphilic nature of these molecules; therefore, the hydrophobic character of the drug was modified. The addition of hydrophobic fatty esters increased the encapsulation efficiency, so we postulated that the long carbon chain may decrease the release rate by making the drug more favorable to the hydrophobic core.<sup>43, 44</sup> The fatty acid prodrugs are susceptible to intra- and extra-cellular esterases and hydrolysis, so the parent drug is expected to reform rapidly after the drug is released from micelles.

The in vitro cytotoxicity study showed that both PSMA-targeted and non-targeted empty micelles were not toxic to DU145 cells. This was not unexpected, since both PEG and PCL polymers are already FDA approved for use in humans and PSMAa10 is made of a single stranded oligonucleotide. However, inhibitory effects were observed with IR-820 labeled PEG-PCL micelles. The toxic effect came from the dye, IR-820, which was reported to significantly inhibit cell growth at concentrations greater than 5  $\mu$ M.<sup>34</sup> Therefore, the IR-820 labeled non-targeted and targeted micelles were only used for examining delivery efficiency, and not for further in vivo characterization.

Due to the change of partition and diffusion coefficients, BL05-HA may have lower membrane permeability compared to its parent drug, BL05, and TGX-221. Thus, the passive diffusion rate of the naked drug to the cells could be lower. The micelle formulation significantly improved cellular uptake of BL05-HA. This is because internalization of PEG-PCL micelles can enhance cellular uptake of encapsulated drugs.<sup>45</sup>

We found that encapsulating BL05-HA with PSMA targeted PEG-PCL micelles increased cytotoxicity in LNCaP cells but not in PC3 cells. This can be explained by the enhanced cellular uptake of the carrier by PSMA-positive cells through a receptor-mediated pathway. Cellular uptake of the naked drug is driven by a concentration gradient. After equilibrium is established, no more drug can enter into the cells. The PEGylated surface of the micelles reduces interaction with the cell surface. Therefore, the cytotoxicities of naked drug and the untargeted drug-loaded micelles in LNCaP and PC3 cells were not significantly different. In PSMA positive cells, the receptor mediated transport of PSMA-targeted micelles improved drug delivery into cells. This significantly enhanced cytotoxicity in PSMA-positive cells. Since the expression of PSMA on PSMA-negative cells was extremely low, the effect of PSMA-targeting was not significant ( $p > 0.05$ ).

A two-compartment model was used to describe the pharmacokinetic (PK) disposition of the PEG-PCL micelle formulation. The PK profile showed that the plasma drug concentration declines biexponentially as the sum of distribution and elimination processes. The rapid drug concentration decrease in initial phase was due to the drug's distribution from the central compartment into the peripheral compartments. Drug metabolism and excretion contributed to the gradual decrease in the plasma concentration during the beta phase. In the pharmacokinetics study, we have shown that the PEGylated micelles can increase the plasma AUC and detectable systemic circulation of the drug by avoiding clearance by the reticuloendothelial system (RES) and kidneys. The RES consists primarily of monocytes and macrophages in the spleen and liver that are responsible for clearing molecules bound with serum proteins. The kidneys also clear unbound drugs by glomerular filtration that are below the renal exclusion limit of ca. 20-60 kDa. Stealth nanoparticles surface-modified with PEG can avoid clearance by the RES and kidneys, thus they have prolonged circulation half-lives in the plasma.<sup>46</sup> This approach has been used to optimize pharmacokinetic

disposition of nanoparticles and enhance drug delivery.<sup>46, 47</sup> In this study, the high  $V_d$  value of naked BL05-HA may be due to its high tissue distribution. A rapid total body clearance rate is also apparent. The micelle formulation significantly reduced the  $V_d$  by minimizing non-specific tissue distribution and the drug was consequently retained within the vascular system. This could also reduce toxicity to normal tissues by reducing their exposure to the drug through non-specific distribution.

## Conclusions

The synthesis of TGX-221, the analog BL05, and the BL05-HA and BL05-PA prodrugs were successfully accomplished. Both TGX-221 and its analog BL05 had an inhibitory effect on phosphorylation of Akt in PTEN-deficient LNCaP cells. Encapsulation of BL05-HA in PEG-PCL micelles resulted in sustained release over several days. In vitro, we have shown that micelles targeted with PSMAa10 and loaded with BL05-HA significantly inhibit the growth of PSMA-positive prostate cancer cells but not PSMA-negative cells. In vivo pharmacokinetics demonstrated that PSMA-targeted micelles significantly increased the AUC and decreased the total body clearance rate of the drug. These findings suggest that PSMA-targeted micelles are a promising drug delivery vehicle for developing PI3-kinase inhibitor treatments of PSMA positive prostate cancers. A future study will examine the efficacy of this formulation in xenografts of human prostate cancer.

## Acknowledgments

This work was funded by Congressionally Directed Medical Research Program IDEA Award in Prostate Cancer (KAN0061569), DOD grant W81XWH-09-1-0455 (PI: Benyi Li) and Kansas Academy of Science Graduate Student Research Grant (PI: Yunqi Zhao). We also thank the CCET Synthetic Medicinal Chemistry Laboratory core (NIH P20RR015563, PI: Timmerman) for assistance in the synthesis of the drugs and Dr. Jeffrey Krise for the use of his microscopy equipment.

## References

1. Steelman LS, Chappell WH, Abrams SL, Kempf RC, Long J, Laidler P, Mijatovic S, Maksimovic-Ivanic D, Stivala F, Mazzarino MC, Donia M, Fagone P, Malaponte G, Nicoletti F, Libra M, Milella M, Tafuri A, Bonati A, Basecke J, Cocco L, Evangelisti C, Martelli AM, Montalto G, Cervello M, McCubrey JA. Roles of the Raf/MEK/ERK and PI3K/PTEN/Akt/mTOR pathways in controlling growth and sensitivity to therapy-implications for cancer and aging. *Aging*. 2011; 3(3):192–222. [PubMed: 21422497]
2. Dbouk HA, Backer JM. A beta version of life: p110beta takes center stage. *Oncotarget*. 2010; 1(8): 729–733. [PubMed: 21321382]
3. Qiao M, Sheng S, Pardee AB. Metastasis and AKT activation. *Cell Cycle*. 2008; 7(19):2991–2996. [PubMed: 18818526]
4. Zhang S, Yu D. PI(3)king apart PTEN's role in cancer. *Clin Cancer Res*. 2010; 16(17):4325–4330. [PubMed: 20622047]
5. van Duijn PW, Ziel-van der Made AC, van der Korput JA, Trapman J. PTEN-mediated G1 cell-cycle arrest in LNCaP prostate cancer cells is associated with altered expression of cell-cycle regulators. *The Prostate*. 2010; 70(2):135–146. [PubMed: 19784964]
6. Pore N, Liu S, Haas-Kogan DA, O'Rourke DM, Maity A. PTEN mutation and epidermal growth factor receptor activation regulate vascular endothelial growth factor (VEGF) mRNA expression in human glioblastoma cells by transactivating the proximal VEGF promoter. *Cancer research*. 2003; 63(1):236–241. [PubMed: 12517803]
7. Rameh LE, Cantley LC. The role of phosphoinositide 3-kinase lipid products in cell function. *J Biol Chem*. 1999; 274(13):8347–8350. [PubMed: 10085060]
8. Jia S, Roberts TM, Zhao JJ. Should individual PI3 kinase isoforms be targeted in cancer? *Current opinion in cell biology*. 2009; 21(2):199–208. [PubMed: 19200708]

9. Jia S, Liu Z, Zhang S, Liu P, Zhang L, Lee SH, Zhang J, Signoretti S, Loda M, Roberts TM, Zhao JJ. Essential roles of PI(3)K-p110beta in cell growth, metabolism and tumorigenesis. *Nature*. 2008; 454(7205):776–779. [PubMed: 18594509]
10. Foukas LC, Berenjeno IM, Gray A, Khwaja A, Vanhaesebroeck B. Activity of any class IA PI3K isoform can sustain cell proliferation and survival. *Proc Natl Acad Sci U S A*. 2010; 107(25): 11381–11386. [PubMed: 20534549]
11. Billottet C, Banerjee L, Vanhaesebroeck B, Khwaja A. Inhibition of class I phosphoinositide 3-kinase activity impairs proliferation and triggers apoptosis in acute promyelocytic leukemia without affecting atra-induced differentiation. *Cancer research*. 2009; 69(3):1027–1036. [PubMed: 19176369]
12. Jackson SP, Schoenwaelder SM, Goncalves I, Nesbitt WS, Yap CL, Wright CE, Kenche V, Anderson KE, Dopheide SM, Yuan Y, Sturgeon SA, Prabakaran H, Thompson PE, Smith GD, Shepherd PR, Daniele N, Kulkarni S, Abbott B, Saylik D, Jones C, Lu L, Giuliano S, Hughan SC, Angus JA, Robertson AD, Salem HH. PI 3-kinase p110beta: a new target for antithrombotic therapy. *Nat Med*. 2005; 11(5):507–514. [PubMed: 15834429]
13. Tai W, Shukla RS, Qin B, Li B, Cheng K. Development of a peptide-drug conjugate for prostate cancer therapy. *Mol Pharm*. 2011; 8(3):901–912. [PubMed: 21510670]
14. Laurent A, Mottu F, Chapot R, Zhang JQ, Jordan O, Rufenacht DA, Doelker E, Merland JJ. Cardiovascular effects of selected water-miscible solvents for pharmaceutical injections and embolization materials: a comparative hemodynamic study using a sheep model. *PDA J Pharm Sci Technol*. 2007; 61(2):64–74. [PubMed: 17479714]
15. Sampath P, Brem H. Implantable Slow-Release Chemotherapeutic Polymers for the Treatment of Malignant Brain Tumors. *Cancer Control*. 1998; 5(2):130–137. [PubMed: 10761024]
16. Davis ME, Chen ZG, Shin DM. Nanoparticle therapeutics: an emerging treatment modality for cancer. *Nat Rev Drug Discov*. 2008; 7(9):771–782. [PubMed: 18758474]
17. Jain AK, Das M, Swarnakar NK, Jain S. Engineered PLGA nanoparticles: an emerging delivery tool in cancer therapeutics. *Crit Rev Ther Drug Carrier Syst*. 2011; 28(1):1–45. [PubMed: 21395514]
18. Grimm J, Scheinberg DA. Will nanotechnology influence targeted cancer therapy? *Semin Radiat Oncol*. 2011; 21(2):80–87. [PubMed: 21356476]
19. Arias JL. Drug targeting strategies in cancer treatment: an overview. *Mini Rev Med Chem*. 2011; 11(1):1–17. [PubMed: 21235512]
20. Saha RN, Vasanthakumar S, Bende G, Snehalatha M. Nanoparticulate drug delivery systems for cancer chemotherapy. *Mol Membr Biol*. 2010; 27(7):215–231. [PubMed: 20939772]
21. Gong C, Wei X, Wang X, Wang Y, Guo G, Mao Y, Luo F, Qian Z. Biodegradable self-assembled PEG-PCL-PEG micelles for hydrophobic honokiol delivery: I. Preparation and characterization. *Nanotechnology*. 2010; 21(21):215103. [PubMed: 20431208]
22. Master AM, Rodriguez ME, Kenney ME, Oleinick NL, Gupta AS. Delivery of the photosensitizer Pc 4 in PEG-PCL micelles for in vitro PDT studies. *J Pharm Sci*. 2010; 99(5):2386–2398. [PubMed: 19967780]
23. Li R, Li X, Xie L, Ding D, Hu Y, Qian X, Yu L, Ding Y, Jiang X, Liu B. Preparation and evaluation of PEG-PCL nanoparticles for local tetradrine delivery. *Int J Pharm*. 2009; 379(1):158–166. [PubMed: 19524653]
24. Bramfeldt H, Sarazin P, Vermette P. Characterization, degradation, and mechanical strength of poly(D,L-lactide-co-epsilon-caprolactone)-poly(ethylene glycol)-poly(D,L-lactide-co-epsilon-caprolactone). *J Biomed Mater Res A*. 2007; 83(2):503–511. [PubMed: 17503493]
25. Zhang, H. *Molecular Imaging and Contrast Agent Database (MICAD)*. Bethesda (MD): 2004. Quantum dot-A10 RNA aptamer-doxorubicin conjugate.
26. Chaux A, Eifler J, Karram S, Al-Hussain T, Faraj S, Pomper M, Rodriguez R, Netto G. Focal positive prostate-specific membrane antigen (PSMA) expression in ganglionic tissues associated with prostate neurovascular bundle: Implications for novel intraoperative PSMA-based fluorescent imaging techniques. *Urol Oncol*. 2011

27. Baccala A, Sercia L, Li J, Heston W, Zhou M. Expression of prostate-specific membrane antigen in tumor-associated neovasculature of renal neoplasms. *Urology*. 2007; 70(2):385–390. [PubMed: 17826525]
28. Gala JL, Loric S, Guiot Y, Denmeade SR, Gady A, Brasseur F, Heusterspreute M, Eschwege P, De Nayer P, Van Cangh P, Tombal B. Expression of prostate-specific membrane antigen in transitional cell carcinoma of the bladder: prognostic value? *Clin Cancer Res*. 2000; 6(10):4049–4054. [PubMed: 11051255]
29. Thiel KW, Giangrande PH. Intracellular delivery of RNA-based therapeutics using aptamers. *Ther Deliv*. 2010; 1(6):849–861. [PubMed: 21643487]
30. Prasad BA, Gilbertson SR. One-pot synthesis of unsymmetrical N-heterocyclic carbene ligands from N-(2-iodoethyl)arylamine salts. *Org Lett*. 2009; 11(16):3710–3713. [PubMed: 19624103]
31. Pierri E, Avgoustakis K. Poly(lactide)-poly(ethylene glycol) micelles as a carrier for griseofulvin. *J Biomed Mater Res A*. 2005; 75(3):639–647. [PubMed: 16110497]
32. Jette KK, Law D, Schmitt EA, Kwon GS. Preparation and drug loading of poly(ethylene glycol)-block-poly(epsilon-caprolactone) micelles through the evaporation of a cosolvent azeotrope. *Pharm Res*. 2004; 21(7):1184–1191. [PubMed: 15290858]
33. Decuzzi P, Pasqualini R, Arap W, Ferrari M. Intravascular delivery of particulate systems: does geometry really matter? *Pharm Res*. 2009; 26(1):235–243. [PubMed: 18712584]
34. Mody VV, Siwale R, Singh A, Mody HR. Introduction to metallic nanoparticles. *J Pharm Bioallied Sci*. 2010; 2(4):282–289. [PubMed: 21180459]
35. Sitzia J, North C, Stanley J, Winterberg N. Side effects of CHOP in the treatment of non-hodgkin's lymphoma. *Cancer Nurs*. 1997; 20(6):430–439. [PubMed: 9409065]
36. Yuan JN, Chao Y, Lee WP, Li CP, Lee RC, Chang FY, Yen SH, Lee SD, Whang-Peng J. Chemotherapy with etoposide, doxorubicin, cisplatin, 5-fluorouracil, and leucovorin for patients with advanced hepatocellular carcinoma. *Med Oncol*. 2008; 25(2):201–206. [PubMed: 18488159]
37. Chidambaram M, Manavalan R, Kathiresan K. Nanotherapeutics to overcome conventional cancer chemotherapy limitations. *J Pharm Pharm Sci*. 2011; 14(1):67–77. [PubMed: 21501554]
38. Cho K, Wang X, Nie S, Chen ZG, Shin DM. Therapeutic nanoparticles for drug delivery in cancer. *Clin Cancer Res*. 2008; 14(5):1310–1316. [PubMed: 18316549]
39. Peer D, Karp JM, Hong S, Farokhzad OC, Margalit R, Langer R. Nanocarriers as an emerging platform for cancer therapy. *Nat Nanotechnol*. 2007; 2(12):751–760. [PubMed: 18654426]
40. Marchal C, Redondo M, Padilla M, Caballero J, Rodrigo I, Garcia J, Quian J, Boswick DG. Expression of prostate specific membrane antigen (PSMA) in prostatic adenocarcinoma and prostatic intraepithelial neoplasia. *Histology and histopathology*. 2004; 19(3):715–718. [PubMed: 15168332]
41. Frazzetto M, Suphioglu C, Zhu J, Schmidt-Kittler O, Jennings IG, Cranmer SL, Jackson SP, Kinzler KW, Vogelstein B, Thompson PE. Dissecting isoform selectivity of PI3K inhibitors: the role of non-conserved residues in the catalytic pocket. *Biochem J*. 2008; 414(3):383–390. [PubMed: 18489260]
42. Patrick Lim Soo LL, Maysinger Dusica, Eisenberg Adi. Incorporation and Release of Hydrophobic Probes in Biocompatible Polycaprolactone-block-poly(ethylene oxide) Micelles: Implications for Drug Delivery. *Langmuir*. 2002; 18(25):9996–10004.
43. Forrest ML, Won CY, Malick AW, Kwon GS. In vitro release of the mTOR inhibitor rapamycin from poly(ethylene glycol)-b-poly(epsilon-caprolactone) micelles. *J Control Release*. 2006; 110(2):370–377. [PubMed: 16298448]
44. Forrest ML, Zhao A, Won CY, Malick AW, Kwon GS. Lipophilic prodrugs of Hsp90 inhibitor geldanamycin for nanoencapsulation in poly(ethylene glycol)-b-poly(epsilon-caprolactone) micelles. *J Control Release*. 2006; 116(2):139–149. [PubMed: 16926059]
45. Diao YY, Li HY, Fu YH, Han M, Hu YL, Jiang HL, Tsutsumi Y, Wei QC, Chen DW, Gao JQ. Doxorubicin-loaded PEG-PCL copolymer micelles enhance cytotoxicity and intracellular accumulation of doxorubicin in adriamycin-resistant tumor cells. *Int J Nanomedicine*. 2011; 6:1955–1962. [PubMed: 21976972]
46. Li SD, Huang L. Nanoparticles evading the reticuloendothelial system: role of the supported bilayer. *Biochim Biophys Acta*. 2009; 1788(10):2259–2266. [PubMed: 19595666]



47. Ozcan I, Segura-Sanchez F, Bouchemal K, Sezak M, Ozer O, Guneri T, Ponchel G. Pegylation of poly( $\gamma$ -benzyl-L-glutamate) nanoparticles is efficient for avoiding mononuclear phagocyte system capture in rats. *Int J Nanomedicine*. 2010; 5:1103–1111. [PubMed: 21270961]

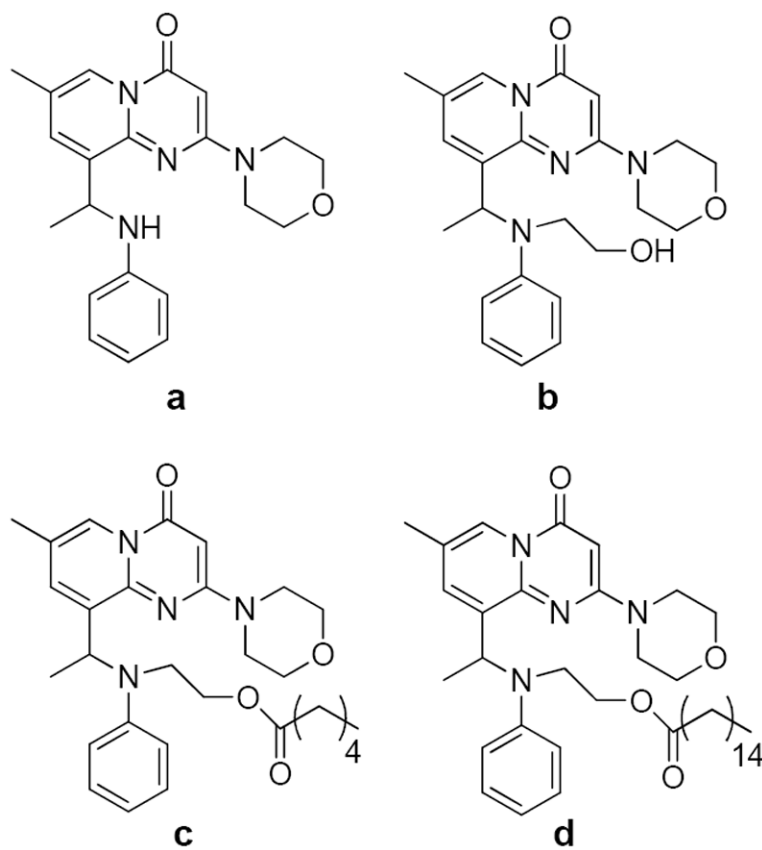


**Figure 1.** Structure of (a) TGX-221; (b) BL05; (c) BL05-HA and (d) BL05-PA.

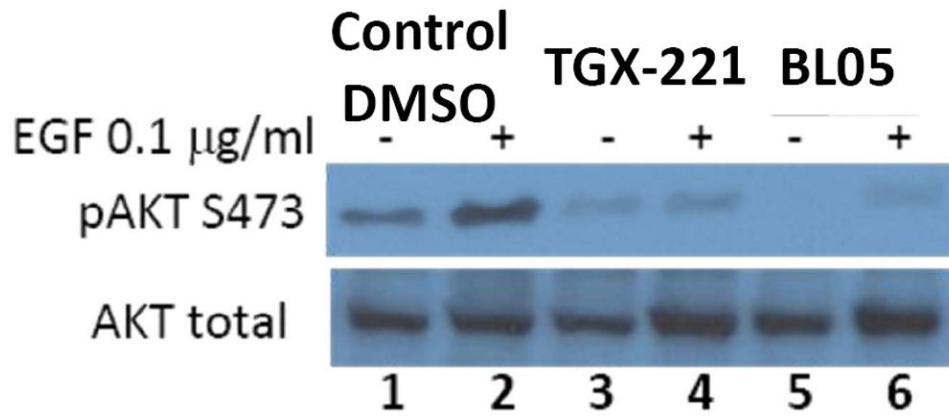


**Figure 2.** Western blot analysis of Akt phosphorylation on Ser473 and total Akt protein levels with different treatments. Both TGX-221 and BL05 showed inhibitory effects on the phosphorylation of Akt.

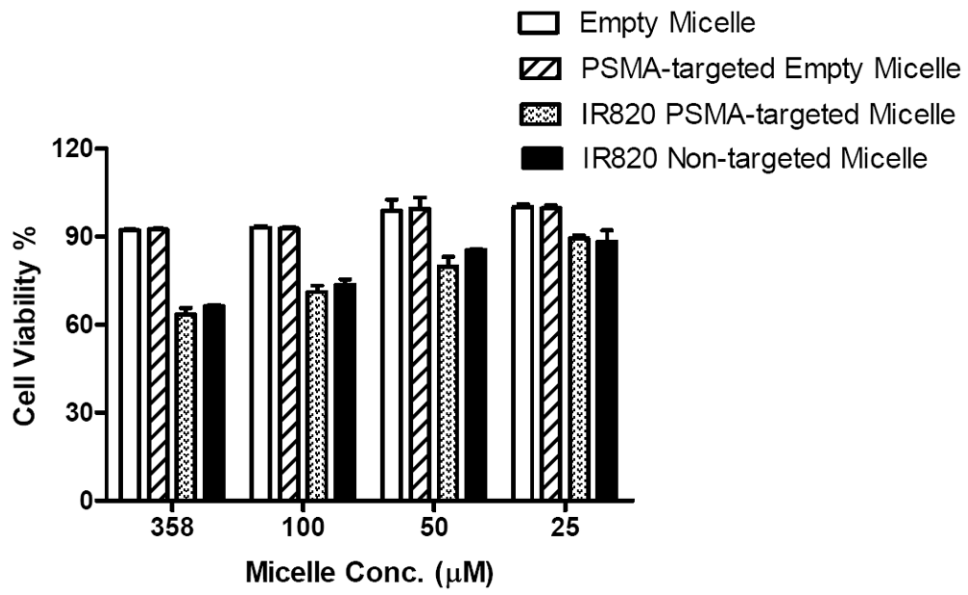


**Figure 3.** Cytotoxicity of empty micelles in DU145 cells (Mean  $\pm$  SD).

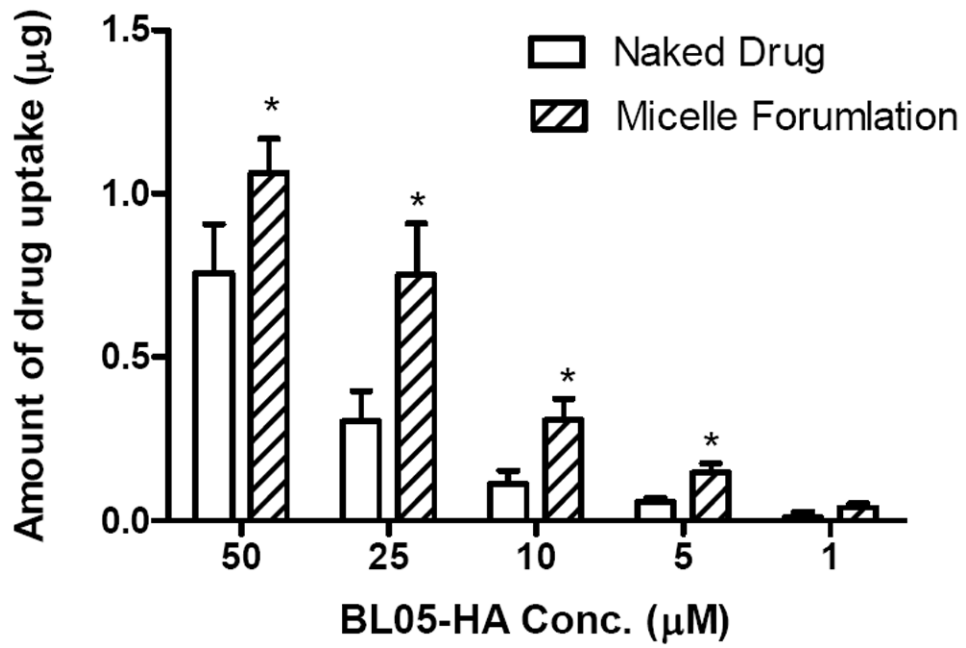


**Figure 4.** The micelle formulation improved DU145's uptake of BL05-HA (Mean  $\pm$  SD). (\*:  $p < 0.001$ )

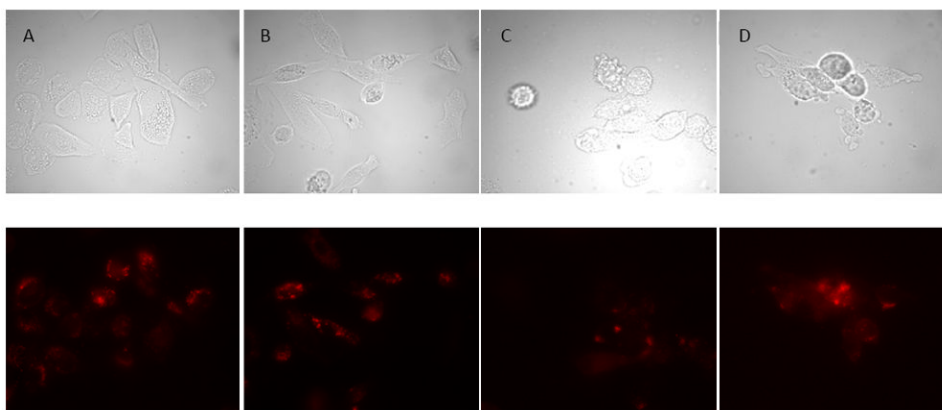
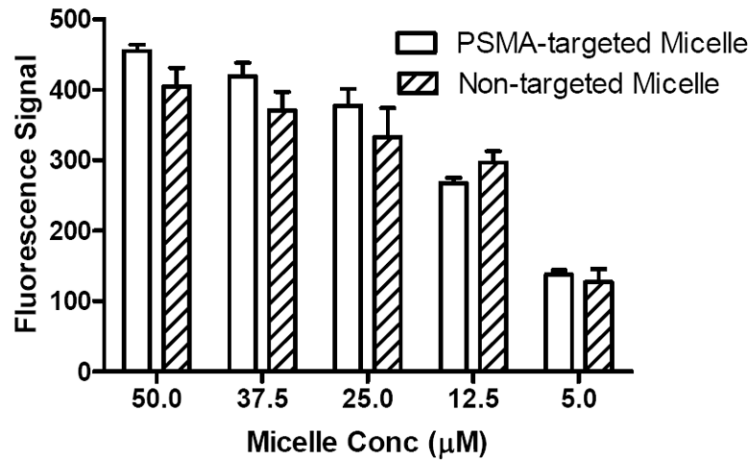
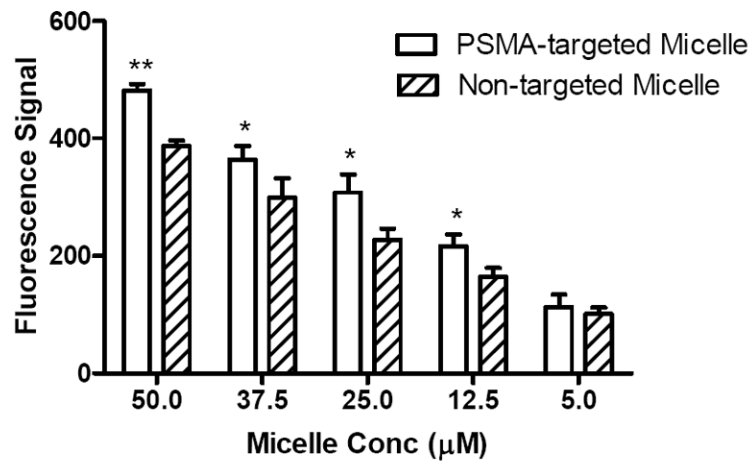


**Figure 5.** Fluorescence imaging study of cell uptake of fluorescent PSMA-targeted micelles in PSMA-positive LNCaP cells. A: PC3 cells treated with non-targeted micelles; B: PC3 cells treated with PSMA-targeted micelles; C: LNCaP cells treated with non-targeted micelles; D: LNCaP cells treated with PSMA-targeted micelles.

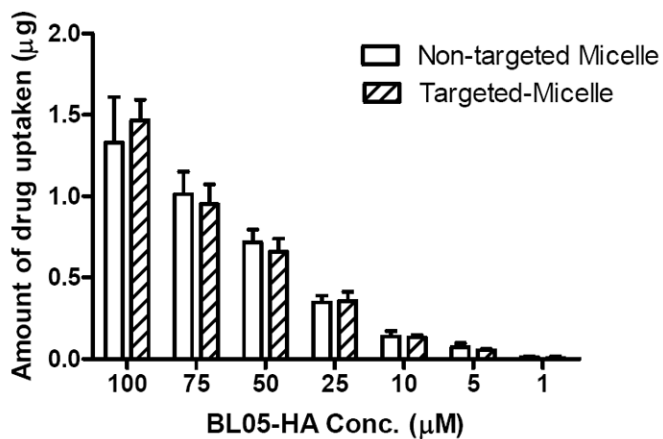


a

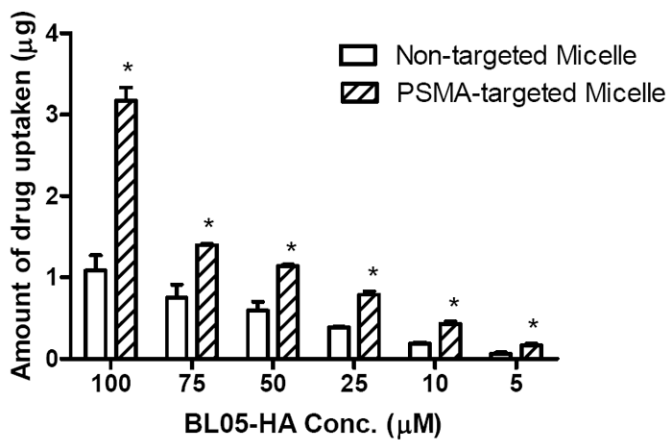


b

**Figure 6.** Uptake of micelles by (a) PC3 cells; and (b) DU145 cells (Mean  $\pm$  SD). (\*:  $p < 0.05$ ; \*\*:  $p < 0.01$ )



a



b

**Figure 7.** PSMA-targeted micelles improved drug uptake by PSMA positive cells. Drug uptake by (a) PSMA-negative DU145 cells and (b) PSMA-positive LNCaP cells treated with targeted or non-targeted formulations (Mean ± SD). (\*:  $p < 0.001$ )



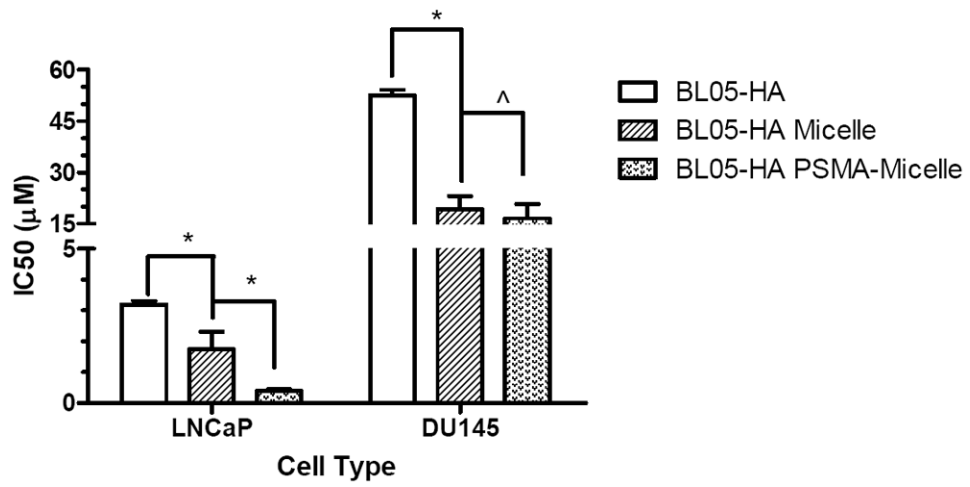


**Figure 8.** IC<sub>50</sub>s of different formulations of BL05-HA in LNCaP and DU145 cells (Mean ± SE). (\*:  $p < 0.01$ ; ^:  $p > 0.05$ )

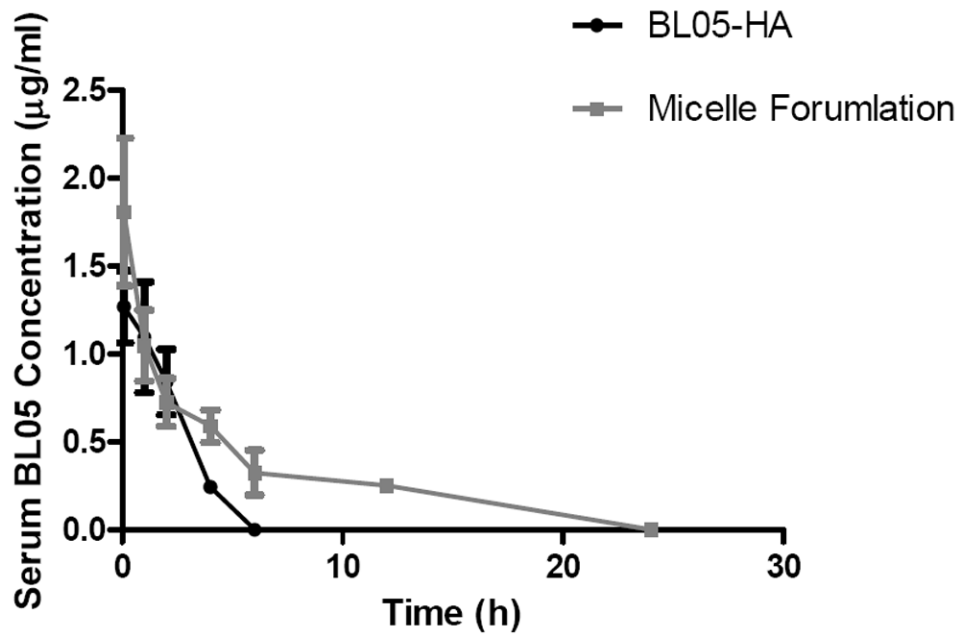
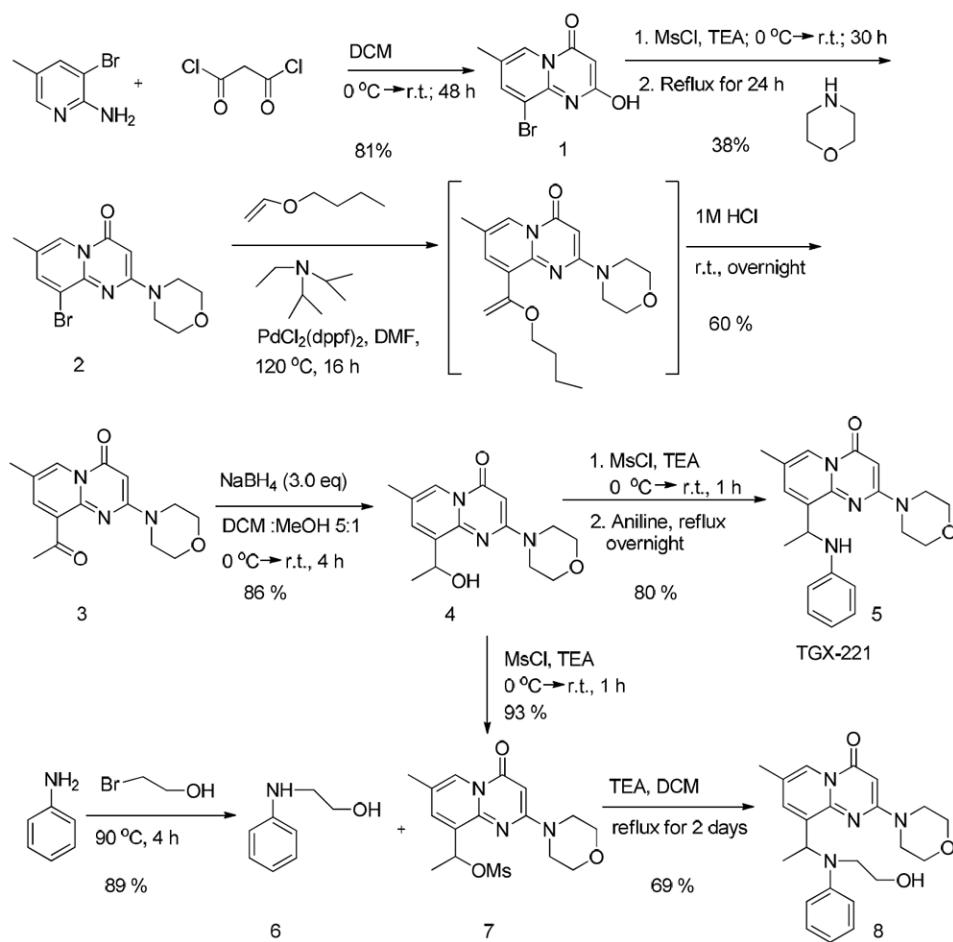


**Figure 9.** Plasma BL05 concentration versus time disposition (Mean  $\pm$  SD) (n = 3).



**Scheme 1.**  
Synthesis of TGX-221 (Compound 5) and BL05 (Compound 8).

**Table 1**

Characterization of different PEG-PCL micelle formulations. All of the formulations had particle sizes that were smaller than 100 nm. The in vitro release half-life was improved by encapsulating more hydrophobic prodrugs.

	Size (nm) (Mean $\pm$ SD)	In vitro Release Half-life
Empty Micelle	27.6 $\pm$ 0.2	-
PSMA-targeted Micelle	40.5 $\pm$ 0.8	-
TGX-221 Loaded Micelle (5% w/w)	54.5 $\pm$ 0.3	<1h
BL05 Loaded Micelle (5% w/w)	59.8 $\pm$ 2.2	< 1 h
BL05-HA Loaded Micelle (5% w/w)	49.9 $\pm$ 0.5	5 days
BL05-PA Loaded Micelle (5% w/w)	29.9 $\pm$ 0.1	6.5 days
BL05-HA Loaded PSMA-targeted Micelle	58.8 $\pm$ 0.9	-

**Table 2**

IC50 of TGX-221, BL05 and BL05-HA in different prostate cancer cell lines. All of the drugs showed selective cytotoxicity to PSMA-positive LNCaP cells. (n=6)

	TGX-221 ( $\mu\text{M}$ ) (Mean $\pm$ SE)	BL05 ( $\mu\text{M}$ ) (Mean $\pm$ SE)	BL05-HA ( $\mu\text{M}$ ) (Mean $\pm$ SE)
<b>DU145</b>	35.6 $\pm$ 0.12	32.4 $\pm$ 0.67	52.5 $\pm$ 0.15
<b>PC3</b>	18.2 $\pm$ 0.85	23.4 $\pm$ 0.74	21.8 $\pm$ 0.66
<b>LNCaP</b>	3.98 $\pm$ 0.18	4.036 $\pm$ 0.11	3.19 $\pm$ 0.12

**Table 3**

Pharmacokinetic parameters after i.v. administration of BL05-HA loaded PSMA-targeted micelles and naked BL05-HA (Mean  $\pm$  SD) (n = 3).

Parameters	Unit	PSMA-targeted Micelle	Naked BL05-HA
$V_d$	mL	0.114 $\pm$ 0.019 <sup>**</sup>	0.160 $\pm$ 0.024
$C_0$	$\mu\text{g}\cdot\text{mL}^{-1}$	1.809 $\pm$ 0.420 <sup>*</sup>	1.270 $\pm$ 0.207
AUC <sub>0-24h</sub>	$\mu\text{g}\cdot\text{h}\cdot\text{mL}^{-1}$	7.682 $\pm$ 0.784 <sup>***</sup>	3.385 $\pm$ 0.290
$k$	$\text{h}^{-1}$	0.647 $\pm$ 0.081 <sup>***</sup>	2.847 $\pm$ 0.083
$k_{12}$	$\text{h}^{-1}$	2.174 $\pm$ 0.749	-
$k_{21}$	$\text{h}^{-1}$	0.698 $\pm$ 0.195	-
Cl	$\text{mL}\cdot\text{h}^{-1}$	0.026 $\pm$ 0.002 <sup>***</sup>	0.455 $\pm$ 0.066

\*  $p < 0.05$ ;

\*\*  $p < 0.01$ ;

\*\*\*  $p < 0.001$